Numerical simulation of surface-plasmon-assisted nanolithography

D. B. Shao and S. C. Chen

Department of Mechanical Engineering, the University of Texas at Austin, Austin, Texas 78712
scchen@mail.utexas.edu

Abstract: In this paper, based on numerical study using Finite Difference Time Domain method, we discuss two possible illumination schemes utilizing surface plasmon effects to achieve high density sub-100 nm scale photolithography by using ultraviolet light from a mercury lamp. In the illumination schemes discussed in this paper, a thin film layer, named as shield layer, is placed in between a photoresist layer and a silicon substrate. In the first scheme, the shield material is titanium. Simulations show that the surface plasmons excited on both the metallic mask and the titanium shield enable the transfer of high density nanoscale pattern using mercury lamp emission. In the second scheme, a silicon dioxide layer is used instead of the titanium to avoid possible metal contamination. The two schemes discussed in this paper offer convenient, low cost, and massive pattern transfer methods by simple adjustment to the traditional photolithography method.

OCIS codes: (220.3740) Lithography, (240.6680) Surface plasmons.

References and links

1. S. Okazaki, "Resolution limits of optical lithography," J. Vac. Sci. Technol. B **9**, 2829-2833 (1991).
2. R. Kunz, M. Rothschild and M. S. Yeung, "Large-area patterning of ~50 nm structures on flexible substrates using near-field 193 nm radiation," J. Vac. Sci. Technol. B **21**, 78 (2003).
3. J. G. Goodberlet and H. Kavak, "Patterning Sub-50 nm features with near-field embedded-amplitude masks," Appl. Phys. Lett. **81**, 1315 (2002).
4. H. Schmid, H. Biebuyck, B. Michel and O. J. F. Martin, "Light-coupling masks for lensless, sub-wavelength optical lithography," Appl. Phys. Lett. **72**, 2379 (1998).
5. M. M. Alkaisi, R. J. Blaikie, S. J. McNab, R. Cheung, and D. R. S. Cummingb, "Sub-diffraction-limited patterning using evanescent near-field optical lithography," Appl. Phys. Lett. **75**, 3560 (1999).
6. T. W. Ebbesen, H. J. Lezec, H. F. Ghaemi, T. Thio, and P. A. Wolff, "Extraordinary optical transmission through sub-wavelength hole arrays," Nature (London) **391**, 667-669 (1999).
7. L. Salomon, F. Grillot, A. V. Zayats and F. de Fornel, "Near-field distribution of optical transmission of periodic subwavelength holes in a metal film," Phys. Rev. Lett. **86**, 1110 (2001).
8. D. E. Grupp, H. J. Lezec, T. W. Ebbesen, K. M. Pellerin and T. Thio, "Crucial role of metal surface in enhanced transmission through subwavelength apertures," Appl. Phys. Lett. **77**, 1569 (2000).
9. H. Raether, "Surface Plasmons on Smooth and Rough Surfaces and on Gratings," Berlin, 1988.
10. J. B. Pendry, "Playing tricks with light," Science **285**, 1687-1688 (2002).
11. E. Popov, M. Nevie`re, S. Enoch, and R. Reinisch, "Theory of light transmission through subwavelength periodic hole arrays," Phys. Rev. B. **62** 16100 (2000).
12. W. Srituravanich, N. Fang, C. Sun, Q. Luo, and X. Zhang, "Surface Plasmonic Lithography," Nano Lett. **4**, 1085 (2004).
13. X. Luo, T. Ishihara, "Surface plasmon resonant interference nanolithography technique," Appl. Phys. Lett. **84**, 4780 (2004).
14. J. B. Pendry, "Negative refraction makes a perfect lens," Phys. Rev. Lett. **85**, 3966 (2000).
15. D.B. Shao, S.C. Chen, "Surface-Plasmon-Assisted Nanoscale Photolithography by Polarized Light," Appl. Phys. Lett. **86**, 253107 (2005).
16. K. S. Yee, "Numerical solution of initial boundary value problems involving Maxwell's equations in isotropic media," IEEE Trans. Antennas Propag. **14**, 302, May 1966.

#8088 - $15.00 USD Received 11 July 2005; revised 24 August 2005; accepted 24 August 2005

17. J. T. Krug II, E. J. Sa´nchez, and X. S. Xie, "Design of Near-field Optical Probes with Optimal Field Enhancement by Finite Difference Time Domain Electromagnetic Simulation," J. Chem. Phys. **116**, 10895 (2002).
18. J. P. Berenger, "A Perfectly Matched Layer for the Absorption of Electromagnetic Waves," J. Comput. Phys. **114**, 185 (1994).
19. S. K. Gray and T. Kupka, "Propagation of light in metallic nanowire arrays: Finite-difference time-domain studies of silver cylinders," Phys. Rev. B **68**, 045415 (2003).
20. E. D. Palik, "Handbook of optical constants of solids," Academic Press, Orlando, 1985.
21. P. W. Barber, S. C. Hill, "Light Scattering by Particles: Computational Methods," World Scientific, Singapore, 1990.

1. Introduction

Photolithography has been the key technique in semiconductor manufacturing and micro-fabrication over the past several decades because of its high throughput, low cost, simplicity, and reproducibility. The traditional photolithography is limited by the illumination wavelength due to the optical diffraction limit[1]. Based on standard diffraction theory, sub-wavelength aperture transmits light poorly and diffracts light in all direction uniformly. Transmission and diffraction have been the fundamental constraints in manipulating light at a sub-wavelength scale. There are growing interests in developing sub-wavelength lithography techniques to fabricate nanoscale devices for nanotechnology applications, however many of the existing nanoscale lithography techniques like electron beam lithography and deep ultraviolet (UV) lithography require expensive additional equipment and cannot meet industrial mass fabrication needs.

With the development of research in near field optics, many sub-wavelength lithography approaches have been proposed in the realm of near-field optical lithography, which replaces the mask in traditional photolithography process with a mask having sophisticatedly designed nanostructures to achieve certain sub-wavelength patterns. In Phase Shift Mask (PSM) method, the mask is made of fused silica with etched gaps, the thickness of which introduces π phase shift due to the difference of optical path length[2], resulting in a local high intensity of light. In Embedded-Amplitude Mask[3] (EAM) method, the mask has three different layers including an embedded metal layer to enhance contrast. The Light Coupling Mask (LCM)[4] approach utilized the fact that light can cross an interface of two materials having matched refractive indices. The Evanescent Near-Field Optical Lithography (ENFOL)[5] method used NiCr patterns on silicon nitride membrane as mask to ensure intimate contact. The near-field optical lithography can be easily adopted in traditional photolithography and inherits the merits of high throughput and low cost. However the process needs deep UV illumination to achieve sub-100 nm features and the common drawbacks are low contrast and complex mask fabrication. Besides, it is still difficult to achieve high-density patterns.

Surface plasmon phenomenon has been known for decades and it stimulated extensive research interests recently since the discovery of the extraordinarily high transmission through sub-wavelength hole arrays on a metal film[6-8]. Surface plasmon represents electromagnetic surface waves that have maximum intensity at the surface and an exponentially decaying field perpendicular to the surface[9]. The coupling of surface plasmon with photons leads to many exciting development in photonics and optical engineering. In the example of the extraordinarily high transmission through perforated metal film, the strong surface electromagnetic (EM) mode, characteristic of metals, can couple to external transverse radiation, dramatically enhancing the transmission of light through sub-wavelength apertures in a metal film[10]. The observed far-field transmission is orders of magnitude higher than predicted by aperture theory[6]. The transmissivity appears to be a function of hole diameter, periodicity of holes, as well as wavelength[6]. The transverse electric (TE) and transverse magnetic (TM) modes usually have different cut-off frequencies when the aperture width is small[11].

#8088 - $15.00 USD Received 11 July 2005; revised 24 August 2005; accepted 24 August 2005

Most recently, the surface plasmon effects have been used for nanoscale photolithography. Srituravanich *et al.*[12] applied a thin layer of SU-8 photoresist behind an aluminum film perforated with a two-dimensional hole array. Array of dots of 90 nm in diameter and 170 nm in period were formed on the photoresist using UV lamp illumination. Luo et al.[13] spun photoresist on a silicon substrate. The surface plasmon excited by a wavelength of 436 nm on the exit side of the silver mask redistributes the light into a sub-100 nm scale interference pattern. However, arbitrary one-to-one pattern transfer has not been achieved yet.

On the other hand, researchers have noticed that surface plasmons on some metal films can focus the EM waves from a near-field object to the opposite side with a resolution far beyond diffraction limit[14]. This finding motivated us to combine the surface plasmon effects on both perforated metal film and planar metal film for nanolithography. In our previous work[15], we have demonstrated Surface Plasmon Assisted Nano-lithography (SPAN) by placing a thin titanium layer ("shield layer") between the photoresist and the silicon substrate illuminated by a laser beam. Our mask was made directly by patterning metal film on quartz substrate without any etching or multi-layer structure. Array of ~100 nm lines with periodicity of 1 μm or 500 nm were obtained to demonstrate the SPAN process. Our Finite Difference Time Domain (FDTD) modeling has provided fairly accurate predictions of the photoresist line profile for different configurations. The simulation also helped in understanding the importance of the surface plasmon in the lithography process. The surface plasmon excited on the mask enhances the light through the sub-wavelength aperture while the surface plasmon excited on the shield layer helps to confine the light intensity to the space behind the mask aperture by coupling. However there are still some issues remaining for the SPAN process. In this paper, we employ FDTD simulation to study the possibility of high density arbitrary pattern transfer at sub-100 nm with mercury lamp illumination. Since the titanium shield layer may raise concerns of metal contamination for some biological or semiconductor applications, we also investigate an alternative scheme to avoid the contamination issue by using a silicon dioxide layer.

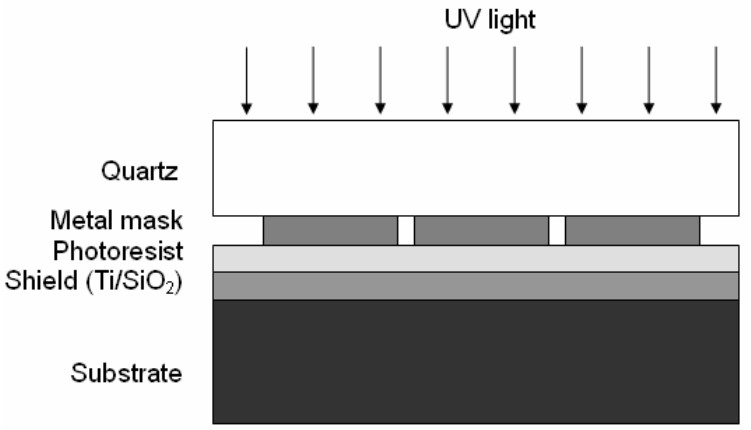

Fig. 1. A schematic view of the SPAN photolithography illumination setup.

2. Numerical simulations

The illumination scheme for SPAN is illustrated in Fig. 1. The results of photolithography depend on the light intensity distribution in the photoresist, which has a threshold energy density for the photochemical reactions to take place. In this paper we use the FDTD method to predict the light intensity distribution in the photoresist. The FDTD method solves the Maxwell's equations and it became feasible after Yee's elegant discretization algorithm[16]. Since then it has been widely used as a fundamental tool in microwave engineering and

#8088 - $15.00 USD Received 11 July 2005; revised 24 August 2005; accepted 24 August 2005

recently FDTD finds its way into near-field optics, such as solving EM fields in the near-field scanning optical microscopy (NSOM)[17].

In nanolithography, the line width is the most important parameter and the present application has long parallel grating structures. Thus a two-dimensional FDTD approach is adequate for our purpose. For a TM mode, the Maxwell's equations reduce to:

$$\begin{aligned}
\varepsilon \frac{\partial E_x}{\partial t} &= \frac{\partial H_z}{\partial y} - \sigma E_x \\
\varepsilon \frac{\partial E_y}{\partial t} &= -\frac{\partial H_z}{\partial x} - \sigma E_y \\
\mu \frac{\partial H_z}{\partial t} &= -(\frac{\partial E_y}{\partial x} - \frac{\partial E_x}{\partial y}) - \sigma^* H_z
\end{aligned} \tag{1}$$

where E and H are electric and magnetic fields respectively, and ε, μ and σ are the permittivity, permeability and electric conductivity of the material, respectively.

Since the Maxwell's equations are wave equations in nature, appropriate boundary conditions must be imposed in order to simulate an 'open space' situation without having any reflected waves from the boundary of computational domain. The Perfectly Matched Layer (PML) method[18], first implemented by Berenger, is applied in our numerical model, in which the magnetic fields in PML are sophisticatedly broken down into two subcomponents to absorb electromagnetic waves outgoing at different angles.

The dielectric constants of metals at optical frequencies are complex numbers because of the absorption, and in most cases the real part of the dielectric constants are negative. This makes the standard time iteration scheme of FDTD method unstable. In our numerical model, a current density term becomes explicit after introducing the Drude model:

$$\varepsilon_D(\omega) = \varepsilon_\infty - \frac{\omega_D^2}{\omega^2 + i\Gamma_D \omega} \tag{2}$$

which is equivalent to the use of a complex-valued dielectric constant[19], as shown below:

$$\varepsilon_{eff} \frac{\partial E_x}{\partial t} = \frac{\partial H_z}{\partial y} - J_x \tag{3}$$

$$\varepsilon_{eff} \frac{\partial E_y}{\partial t} = -\frac{\partial H_z}{\partial x} - J_y \tag{4}$$

$$\mu_0 \frac{\partial H_z}{\partial t} = -(\frac{\partial E_y}{\partial x} - \frac{\partial E_x}{\partial y}) \tag{5}$$

$$\frac{\partial J_x}{\partial t} = \alpha J_x + \beta E_x \tag{6}$$

$$\frac{\partial J_y}{\partial t} = \alpha J_y + \beta E_y \tag{7}$$

where ε_{eff}, α and β are related to ε_∞, Γ_D and ω_D in Drude model as:

$$\varepsilon_{eff} = \varepsilon_0 \varepsilon_\infty \tag{8}$$

$$\alpha = -\Gamma_D \tag{9}$$

$$\beta = \varepsilon_0 \omega_D^2 \tag{10}$$

The optical properties of the metals were first obtained from literature[20] and fitted with the Drude model to determine the constants. In order to verify the validity of the program, the FDTD code was benchmarked with the two-dimensional theoretical solutions of the scattering of light by a cylinder[21]. Fig. 2 compares the field intensities along the two axes of a cylinder calculated by both the theoretical solutions and our FDTD model.

#8088 - $15.00 USD Received 11 July 2005; revised 24 August 2005; accepted 24 August 2005

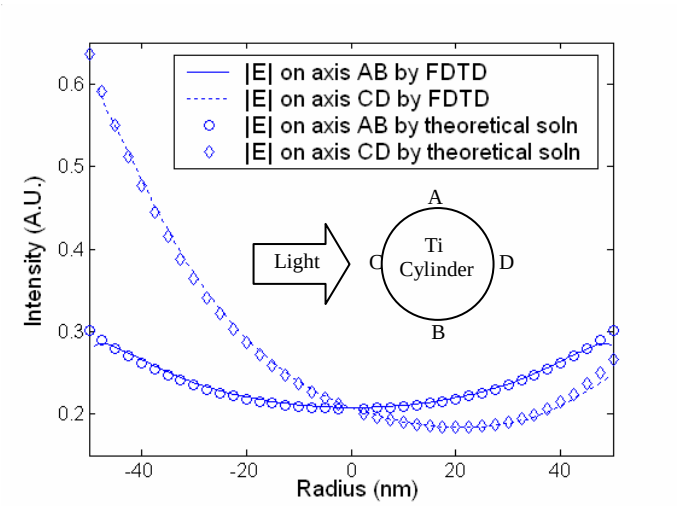

Fig. 2. Comparison of electric field distribution on the axes parallel and perpendicular to the incident light by FDTD simulation and theoretical solution. The incident light wavelength is 365 nm and the cylinder has a diameter of 100 nm.

By integrating the current going in and out of each cell, the charge density distribution can be evaluated, which, as expected, only has non-zero values at the interface of metal and dielectric. The time harmonic charge oscillation at the metal-dielectric interface shows the surface plasmon effect and leads to the understanding of the coupling between the light and the surface plasmon.

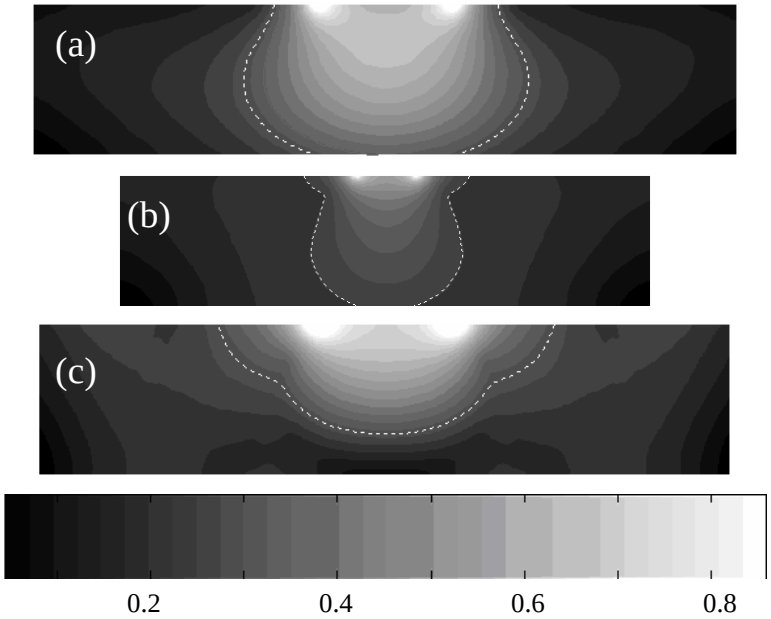

Fig. 3. Electric field distribution in the photoresist with: (a) a Ti mask and Ti shield, 50 nm aperture, and 60 nm resist thickness, (b) a Ti mask and Ti shield, 20 nm aperture, and 50 nm resist thickness, (c) a Ti mask and bare silicon substrate, 50 nm aperture and 60 nm resist thickness. The dotted line represents intensity contour at ~40% incident light intensity.

#8088 - $15.00 USD Received 11 July 2005; revised 24 August 2005; accepted 24 August 2005

3. Results and discussion

The ultraviolet light from the mercury lamp has a spectrum with several peaks and the maximum peak is centered at 365 nm with a full width at half maximum (FWHM) of about 20 nm. The wide emission spectrum made the photolithography using mercury lamp quite complex, especially for a silicon substrate. Although the optical properties of metals, for example titanium, do not vary significantly across the UV range (refractive index 1.3 at 354 nm and 1.44 at 376 nm, extinction coefficient 2.01 at 354 nm and 2.09 at 376 nm)[20], the optical properties of silicon change dramatically (refractive index 5.61 at 354 nm and 6.71 at 376 nm, extinction coefficient 3.01 at 354 nm and 1.32 at 376 nm) [20]. Since the optical penetration depth of UV light in titanium is only about 30 nm, we believe that by using a titanium shield layer of approximately 60 nm the variation of optical properties of silicon across the UV emission spectrum should not be an issue any more. Here we show our simulation results at 365 nm, the peak emission wavelength of mercury lamp. The photoresist in our model has a refractive index of 1.67, as that of SU-8, a commonly used negative photoresist. The aperture width is also reduced to observe the changes in the electric field distribution.

Figure 3 shows the electric fields contour in the photoresist layer with different configurations. In Fig. 3(a), the aperture width is 50 nm and the photoresist has a thickness of 60 nm. In this case we used a titanium mask and titanium shield layer on the substrate. The dotted line is a contour that has 40% of the maximum intensity, which could roughly represent the profile of the photoresist line at appropriate illumination intensity. In Fig. 3(b), the mask aperture width is further reduced to 20 nm and the photoresist has a thickness of 50 nm. Light confinement is still achieved behind the 20 nm aperture, however it should be noted that the light transmission is significantly reduced. The maximum intensity inside the photoresist is only about 60% as compared to that in Fig. 3(a), with the same illumination intensity. Fig. 3(c) has the same configuration as that of Fig. 3(a) but without a shield layer. Since the refractive index of silicon is much larger than that of the photoresist, a great portion of the electromagnetic wave is reflected back with a π-phase difference that interferes with the incoming wave. The low intensity electric field at the interface makes the photoresist lines significantly broadened, since the light intensity has to be high enough in order to photo-initiate the resist at the interface.

When the plane wave encounters the metal shield layer, the electric fields, E_x and E_y, drive the free electrons in the shield and produce a harmonically oscillating surface charge at the surface. The charges are having symmetric amplitude but opposite signs across the centerline of the aperture, as shown in Fig. 4. The opposite charges in turn produce an electric field that counter-acts on the incoming electric field. This strongly helps in preventing the interaction of adjacent electric fields exiting from neighboring apertures and thus high density patterning becomes feasible. In Fig. 3(a), the apertures have a periodicity of 300 nm. The periodicity can be further decreased until the surface plasmons excited on the shield layer start to interfere with each other, as shown in Fig. 4, which has 150 nm periodicity. Below the 150 nm periodicity, FDTD simulations show that the light intensity inside the resist starts to lose contrast.

#8088 - $15.00 USD Received 11 July 2005; revised 24 August 2005; accepted 24 August 2005

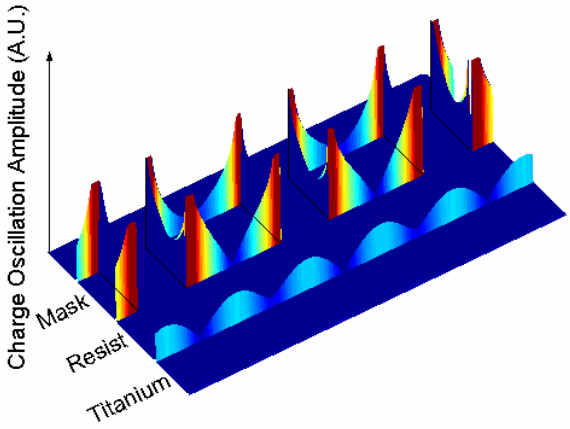

Fig. 4. Charge oscillation amplitude distribution with Ti mask and Ti shield.

In our simulations, an array of five apertures was constructed in the model. Aperture arrays with different periodicity as well as with different number of apertures were also tested. The light intensity behind each slit is not uniform and varies slightly at different locations. However the variation is not as significant as reported for a perforated metal film[6]. We believe the presence of titanium shield layer results in the difference and is the key for the possible high density arbitrary pattern transfer. Since the UV emission spectrum from a mercury lamp has several other peaks away from 365 nm, a band pass filter centered at 365 nm is recommended for this illumination scheme using broadband light. The FWHM of such a filter could be as wide as 50 nm to allow only the main peak of the UV light to transmit.

While the above illumination scheme is very useful to many nanoscale device fabrication applications, the metal layer on the substrate is prohibited in some cases, especially for semiconductor applications. Hence, we also investigated the use of a silicon dioxide layer of tens of nanometers in thickness as the “shield layer”. Silicon dioxide is a common semiconductor material and the reason for using such a thin layer is to leave the above mentioned low intensity area away from the photoresist layer. To further reduce the contamination issue, a thin layer of PMMA (refractive index = 1.5 at 365 nm) is spun on the mask to avoid direct contact of the metal mask to the photoresist.

After investigation of many configurations, we found an illumination scheme at 365 nm wavelength. The metal mask is titanium with thickness of 40 nm and a 70 nm PMMA layer covers the metal mask. A 40 nm silicon dioxide film is grown on the Si substrate. From the electric field contour in Fig. 5(a), we can see that the light intensity distribution in the dioxide layer is distorted. However the light intensity contour in the photoresist still meets the requirement for lithography. It can also be seen that the contour line has a width noticeably larger than the aperture width in this case, as compared to the situation in Fig. 3(a). Our FDTD simulations also show that 10 nm variation in the geometry dimensions, such as the thickness of PMMA or silicon dioxide could be tolerable. As a comparison, Fig. 5(b) shows the electric field contour with a mask made of chromium since chromium is the most common mask material.

#8088 - $15.00 USD Received 11 July 2005; revised 24 August 2005; accepted 24 August 2005

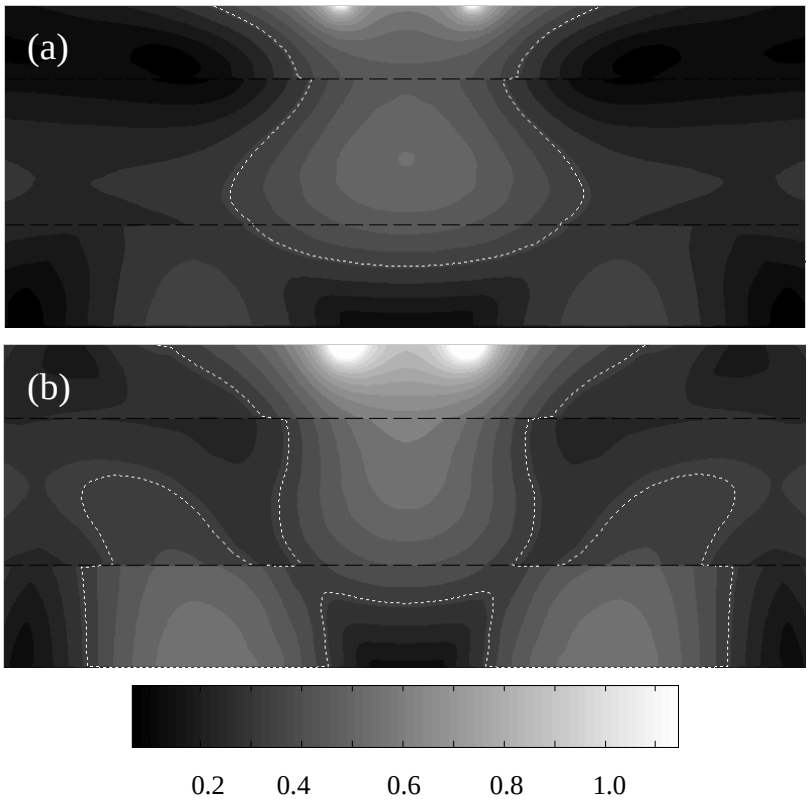

Fig. 5. Electric field distribution in the photoresist with: (a) Ti mask and SiO2 layer, (b) Cr mask and SiO2 layer. Mask aperture is 50 nm. The silicon dioxide layer has a thickness of 40 nm. The dotted line represents intensity contour at ~40% incident light intensity. The dashed line defines the interface of PMMA and resist, resist and silicon dioxide.

In the second scheme the high intensity electric fields behind the adjacent apertures tend to interact with each other without the coupling effect from surface plasmon. From simulations we found that a minimum periodicity of 300 nm is required in order to have enough contrast for lithography. Moreover, the silicon substrate is exposed to the illumination light and the electric field distribution becomes sensitive to the illumination wavelength. We carried out FDTD simulations at wavelengths of 354 nm and 376 nm respectively. Figures 6(a) and 6(b) plot the intensity in the lateral direction at different heights from the bottom of the photoresist layer for the two wavelengths. While there are no obvious changes in the contours at the 354 nm wavelength, the electric field intensity for the 376 nm wavelength is significantly flattened. Considering the wide spectrum emission from a mercury lamp, it will be difficult to achieve fine photolithography results directly using the UV light from a mercury lamp. Based on this consideration, a narrow band pass filter (~10 nm FWHM) is recommended for this scheme.

#8088 - $15.00 USD Received 11 July 2005; revised 24 August 2005; accepted 24 August 2005

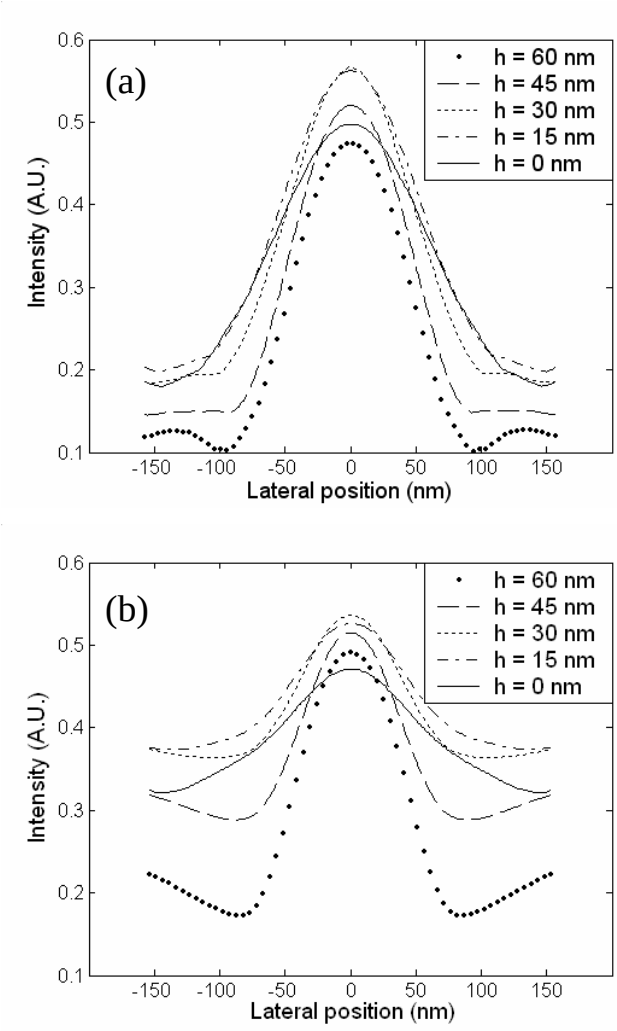

Fig. 6. Electric field plot at different heights within the photoresist with Ti mask and silicon dioxide layer at (a) 354 nm wavelength and (b) 376 nm wavelength.

Surface plasmon varies its behavior in different metals when coupled to the surrounding EM fields and could affect the near-field distribution differently. Titanium happens to be the optimal choice of mask in the two schemes we discussed in this paper. In other configurations however, metals such as Ag could be a better candidate for light localization. The complex configuration as well as the nonlinear behavior of the EM fields makes it hard to predict without FDTD simulations. We believe the SPAN process is capable of achieving 20 nm resolution for lithography with precise control of the illumination light intensity. However, a 10 nm resolution will be a turning point since the dielectric functions of the materials may start to break down. The dielectric constants of material do not arise from a single atom or molecule but from a collection of them. At the 10 nm scale the dielectric constants of metals will be so deviated that FDTD simulation results could become meaningless.

In summary, we have discussed two lithography schemes for the SPAN process by using a mercury lamp as the light source. The two schemes are complementary to each other in terms of the capability to achieve a high density sub-50 nm line width and avoid potential

#8088 - $15.00 USD Received 11 July 2005; revised 24 August 2005; accepted 24 August 2005

contamination. The SPAN process provides a convenient route for high throughput nanoscale pattern transfer without expensive equipments or complex mask fabrication.

The authors would like to thank Drs. Heinz Schmid and Stephen Gray for their helpful inputs. This work was partially supported by research grants from the US National Science Foundation (Grant Nos. DMI 0222014 and CTS 0243160).

#8088 - $15.00 USD Received 11 July 2005; revised 24 August 2005; accepted 24 August 2005